BIOCHEMISTRY
including biophysical chemistry & molecular biology
Article

Biochemistry **2009,** *48,* 9677–9683 9677
DOI: 10.1021/bi901197c

Primary Reaction of Sensory Rhodopsin II Mutant D75N and the Influence of Azide[†]

Mirka-Kristin Verhoefen,[‡] Martin O. Lenz,[‡] Sergiu Amarie,[‡] Johann P. Klare,[§,∥] Jörg Tittor,[⊥] Dieter Oesterhelt,[⊥] Martin Engelhard,[§] and Josef Wachtveitl*[,‡]

[‡]*Institute of Physical and Theoretical Chemistry, Institute of Biophysics, Johann Wolfgang Goethe-University Frankfurt, Max von Laue-Strasse 7, 60438 Frankfurt am Main, Germany,* [§]*Max-Planck-Institute of Molecular Physiology, Otto-Hahn-Strasse 11, 44139 Dortmund, Germany, and* [⊥]*Max-Planck-Institute of Biochemistry, Am Klopferspitz 18, 82152 Martinsried, Germany.* [∥]*Present address: Department of Physics, University of Osnabrück, Barbarastrasse 7, 49069 Osnabrück, Germany*

Received July 14, 2009; Revised Manuscript Received September 9, 2009

ABSTRACT: The early steps in the photocycle of sensory rhodopsin II mutant D75N are investigated in a comprehensive study using femtosecond visible pump/probe spectroscopy. An overall slower response dynamics after photoexcitation is observed compared to wild-type sensory rhodopsin II, which is assigned to changed electrostatics and an altered hydrogen-bonding network within the retinal binding pocket. Furthermore, the influence of azide on the primary reaction is analyzed. The addition of azide accelerates the sub-10 ps dynamics of the D75N mutant nearly to reaction rates found in wild-type. Moreover, a further reaction pathway becomes observable in the investigated time range, which is assigned to a previously described K_1 to K_2 transition. The specific acceleration of the early steps seems to be a unique feature of the D75N mutant as similar azide effects do not emerge in analogous azide measurements of wild-type sensory rhodopsin II, bacteriorhodopsin, and the bacteriorhodopsin mutant D85N.

For their photosynthetic, phototactic, and osmotic requirements several archaea (like *Natronomonas pharaonis* or *Halobacterium salinarum*) rely on a set of retinal proteins, which possesses seven transmembrane helices as a common structural motif but are spectrally tuned to optimize the absorption properties and functionality. Up to now, four types of archaeal retinal proteins have been identified: bacteriorhodopsin (BR)[1] (*1*, *2*), halorhodopsin (HR) (*3*, *4*), sensory rhodopsin I (SRI) (*5*), and sensory rhodopsin II (SRII) (*6*, *7*). BR and HR are light driven ion pumps, which transfer a proton or a chloride ion, respectively, across the membrane. BR hereby generates a proton gradient which is used for ATP synthesis, whereas HR is responsible for osmotic balance. The photosensors SRI and SRII are in charge of phototaxis signaling. To mediate the phototactic response, they are bound to a large transducer complex in a 2:2 stoichiometry. The signal transduction between the two domains is a matter of current research (*8*). For SRII from *N. pharaonis* (NpSRII) (*9*, *10*) it is suggested that the signal transfer is triggered by a motion of helix F resulting in a rotational or screw-like motion of the second transmembrane helix (TM2) of the transducer (*9*). However, the crystal structure of intermediates taking part in this process does not show any movement of this helix (*11*), which might be due to crystal packing.

Despite their different functions the available three-dimensional structures of these proteins are strikingly similar, especially with respect to the retinal binding site (*6*, *12*). Seven transmembrane α-helices form a pore structure divided into two half-channels by the retinal, which is bound via a Schiff base to a lysine residue. The all-*trans* to 13-*cis* photoisomerization of the retinal chromophore initiates a photocycle leading to further major conformational changes on a wide range of time scales. The emerging intermediates are termed alphabetically (K, L, M, N, O). The residue providing the proton acceptor and concomitantly the counterion of the protonated retinylidene Schiff base (Asp85 in BR) as well as the proton donor (Asp96 in BR) have a high impact on the general properties of the respective proteins. Within NpSRII the importance of the primary proton acceptor, Asp75, has been demonstrated for many functional aspects (*13*−*17*). Upon Asp to Asn mutation several properties are drastically altered: a large red shift of the ground state absorption maximum in comparison to the wild-type (wt) protein of approximately 20 nm is observed (*16*). The photocycle becomes similar to the one observed for NpSRII wt at pH < 5.5, which is reflected by the loss of the functionally relevant M intermediate (*16*). Although the D75N mutant lacks this intermediate, it still exhibits photophobic response to green−blue light (*17*), what is interpreted in terms of M being not a prerequisite for molecular activation (*13*). It has also been shown that D75 has an impact on the signaling properties of the receptor (*15*). When NpSRII D75 mutants D75A, D75N, and D75Q are complexed with the transducer from *N. pharaonis* (NpHtrII), wt-like high sensitivities to photostimuli are found. However, a complex of the NpSRII D75Q mutant with the transducer of *H. salinarum* (HsHtrII) is fully constitutively active, which highlights the transducer sensitivity to the receptor signal. The present work addresses the functional role of Asp75 of NpSRII for the primary reaction.

Since azide has a great impact on the D75N response to blue light in photostationary current measurements (*16*), additionally the effect of azide on the primary dynamics is investigated. Azide

[†]The DFG provided financial support (SFB 807 and CEF "Macromolecular Complexes").

*To whom correspondence should be addressed. Tel: +49 69 798 29351. Fax: +49 69 798 29709. E-mail: wveitl@theochem.uni-frankfurt.de.

[1]Abbreviations: BR, bacteriorhodopsin; DAS, decay-associated spectrum; NpSRII, sensory rhodopsin from *Natronomonas pharaonis*; HR, halorhodopsin; SRI, sensory rhodopsin I; SRII, sensory rhodopsin II; PR, proteorhodopsin; TM2, second transmembrane helix of transducer; wt, wild-type.

Published on Web 09/09/2009

is mainly known for enhancing the deprotonation and also the reprotonation of the Schiff base (*18*, *19*). Two different theories have been proposed for the mechanism of this azide effect. The first explanation claims a shuttle mechanism in which azide is said to shuttle between the immediate vicinity of the Schiff base and the bulk aqueous phase (*20*, *21*). The second theory by Le Coutre et al. (*22*) ascribes the functionality of azide to changes in the hydrogen-bonding network in the retinal binding pocket. They observed for BR that azide in its anionic form binds near the primary proton acceptor Asp85 and stays deprotonated during the time of protonation of the Schiff base. Therefore, it can serve as proton donor. Interestingly, it was found that azide can restore a hydrogen-bonded network in the cytoplasmic channel, which was absent in the primary proton donor mutant BR D96N. This second interpretation is supported by electron parametric resonance measurements of Steinhoff et al. (*23*), which showed that azide decreases the hydrophobic barrier in the proton transfer channel around both the proton donor and the acceptor.

All results will be discussed in reference to NpSRII wt, BR, and the analogous BR mutant BR D85N.

MATERIALS AND METHODS

Sample Preparation. The NpSRII D75N mutant and NpSRII wt were expressed as described by Schmies et al. (*16*) and Hohenfeld et al. (*7*), respectively. The expression of BR and BR D85N is described in ref *24*. All measurements were performed in 10 mM Tris buffer at pH 8 with 500 mM NaCl and 0.1% *n*-dodecyl *β*-D-maltoside. For the azide samples a concentration of 100 mM azide was obtained by adding appropriate amounts of stock solution (5 M).

Spectroscopic Methods. Steady-state absorption spectra were measured with a Specord S100 spectrophotometer from Analytic Jena using fused silica cuvettes with 1 mm optical path length.

Time-resolved transient absorption measurements in the visible were performed with a home-built setup using a CLARK CPA 2001 laser/amplifier system operating at a central wavelength of 775 nm and a repetition rate of ~1 kHz as a source for ultrashort laser pulses. To excite the samples at the absorption maximum, part of the laser fundamental light was converted employing a home-built noncollinear optical parametric amplifier (NOPA) (*25*), resulting in a excitation wavelength of 520 nm for NpSRII D75N, 500 nm for NpSRII wt, 600 nm for BR D85N, and 550 nm for BR wt, respectively. Excitation pulses were adjusted to energies of ~50 nJ and a focal diameter of approximately 100 μm. Single filament white light pulses (supercontinuum, polarization parallel to excitation) were either generated in a sapphire plate (NpSRII D75N and BR) or a CaF_2 substrate (NpSRII wt and BR D85N) and split into two beams, probe and reference. Data detection was implemented in a referenced scheme using two 42-segment photodiode arrays providing a resolution of 10^{-4} optical density units (*26*). An instrumental response function of ~150 fs was achieved, and a spectral range from 430 to 750 nm was covered. To ensure the exchange of the probed sample volume between individual excitation pulses, the fused silica cuvette with 1 mm optical path length was moved laterally with appropriate speed. The sample concentrations were adjusted to an absorbance of ~0.5 at the excitation wavelength. UV/vis absorption spectra were taken prior to and after the time-resolved experiments to ensure that no long-lived photoproducts or photodegraded proteins were accumulated.

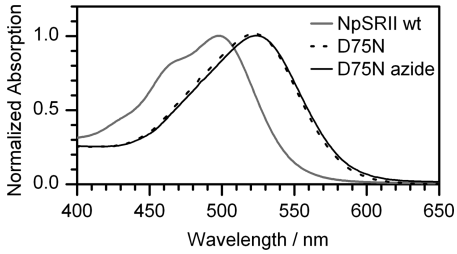

FIGURE 1: Stationary absorption spectra of NpSRII wt and mutant samples: gray, WT; dashed, D75N; black, D75N with 100 mM azide. A red shift of 25 nm for D75N can be seen in comparison to native NpSRII. By adding azide no significant influence on the absorption spectra is observable.

For a quantitative data analysis we employed a kinetic model which describes the experimental data as the sum of exponential decays. A Marquart downhill algorithm optimizes *n* global time constants τ_i for all wavelengths simultaneously with wavelength-dependent amplitudes $A_i(\lambda)$ for each component. Our model function assumes Gaussian pump and probe pulses with a (1/e) cross-correlation width t_{cc}:

$$\Delta A(t,\lambda) = \sum_{i=1}^{n} A_i(\lambda) \exp\left(\frac{{t_{cc}}^2}{4{\tau_i}^2} - \frac{t}{\tau_i}\right) \times \frac{1}{2}\left(1 + \mathrm{erf}\left(\frac{t}{t_{cc}} - \frac{t_{cc}}{2\tau_i}\right)\right)$$

The *n* wavelength-dependent fit amplitudes $A_i(\lambda)$ represent the decay-associated spectra (DAS) for each decay constant. In this definition an infinite time constant is equal to a time-independent offset in the transient absorbance changes, and therefore it mainly corresponds to the signal which remains at the maximum delay time in our experiment (~1.5 ns). The data were corrected for coherent effects around time zero and for group velocity dispersion. Due to the fact that it cannot be excluded that residual contributions of coherent effects remain around time zero, the data analysis was restricted to delay times $t \geq 0.15$ ps.

RESULTS

UV−Vis Absorption Measurements. The UV−vis spectrum of NpSRII D75N depicted in Figure 1 shows a significant red shift of the retinal band of NpSRII D75N (520 nm) compared to NpSRII wt (495 nm). This finding has been reported before by Schmies et al. (*16*) and is in agreement with similar shifts observed for BR and the respective BR D85N mutant (*27*, *28*). The shift is primarily assigned to electrostatic changes in the retinal binding pocket. As can be seen in Figure 1 for the NpSRII D75N mutant the addition of azide does not significantly influence the stationary absorption properties.

Time-Resolved Measurements of NpSRII D75N. Femtosecond time-resolved absorbance changes of NpSRII D75N are shown in Figure 2A. For probing wavelengths between 430 and 750 nm well-resolved contributions in four different spectral regions can be distinguished.

At early delay times an absorption increase at the blue side of the retinal chromophore band is observable (region A in Figure 2A). It can be assigned to the absorption of the first excited state and vanishes on a subpicosecond time scale. For early delay times it overlaps with a negative contribution centered around 520 nm, which can be attributed to the depletion of the ground state (region B in Figure 2A). This negative absorption band shifts slightly to the blue for longer delay times and is centered around 490 nm for delay times > 5 ps. In the region between 550 and 630 nm strong positive absorption changes are observable over the

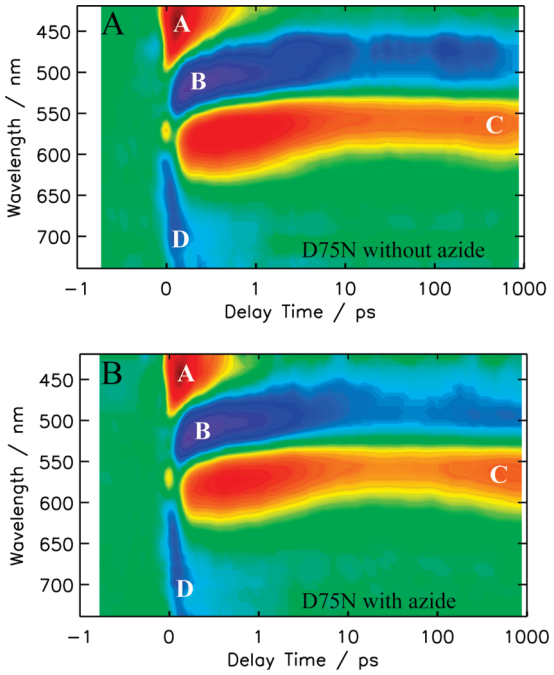

FIGURE 2: Temporal evolution of the transient absorbance changes after photoexcitation at 520 nm of D75N with (A) and without (B) azide. Signal amplitudes are color coded: red labels positive, green neutral, and blue negative absorbance changes. Contributions from excited state absorption (A), ground state bleaching (B), the formation of the red-shifted intermediate (C), and stimulated emission (D) are clearly distinguishable and indicated accordingly in the plot. As for all transients the delay time axis is linear for $\tau < 1$ ps and logarithmic for longer delay times.

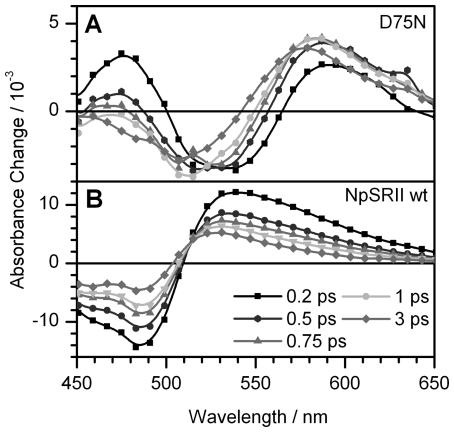

FIGURE 3: Transient absorption spectra at different delay times for NpSRII D75N (A) and wt (B) at pH 8.0. Ground state bleaching and excited state absorption are observable. For the mutant no stationary point is detected, whereas this feature is clearly visible in the wt sample.

whole investigated time range. The signal originates most likely from overlapping contributions of excited state decay and photoproduct formation leading to a constant positive absorption for delay times > 20 ps (region C in Figure 2A). In analogy to NpSRII wt (*29*) the spectral characteristics at 1500 ps are attributed to the $D75N_K$ − D75N spectrum. For wavelengths > 600 nm stimulated emission (region D in Figure 2A) arises within the time resolution of the experiment and decays with the same temporal behavior as the excited state absorption.

Figure 3 shows transient difference spectra of NpSRII D75N (A) and wt (B) at selected delay times between 450 and 650 nm.

Table 1: Comparison of the Global Fit Analysis for Transient Absorption Measurements of NpSRII wt and NpSRII D75N with and without Azide

	τ_1/ps	τ_2/ps	τ_3/ps	τ_4/ps	τ_∞
NpSRII wt[a]	< 0.15	0.3	4−5		infinite
NpSRII D75N	< 0.15	0.8	3.5		infinite
NpSRII D75N azide	< 0.15	0.5	3	450	infinite

[a]Reference *29*.

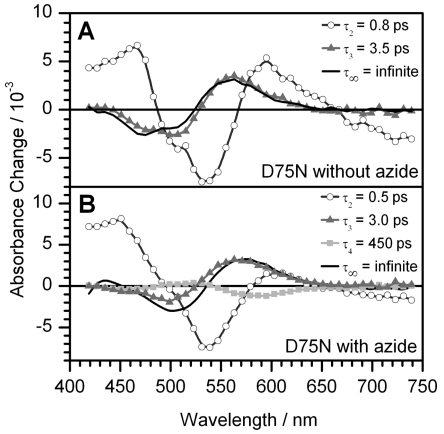

FIGURE 4: Fit amplitudes (DAS) of the multiexponential global fit analysis of D75N without (A) and with (B) 100 mM azide. Spectra for the main time constants are given.

Contributions of excited state absorption (positive signals) and ground state bleaching (negative signals) are observable. Clearly, for the D75N mutant no stationary point can be found as is evidently observed in the transient spectra of NpSRII wt around 510 nm (Figure 3B and ref *29*). Therefore, the early photoreaction of the D75N mutant seems to be more complex than in NpSRII wt.

For further analysis the transient data were analyzed by a global fitting routine, revealing that the data can be satisfactorily described with four time constants ($\tau_1 \leq 0.15$ ps, $\tau_2 = 0.8$ ps, $\tau_3 = 3.5$ ps, and $\tau_\infty \gg 1$ ns, which can be treated as infinity for the time range investigated here; Table 1). The shortest decay time constant τ_1 is in the range of the time resolution of this measurement and hence is obscured by coherent effects due to the temporal overlap of the pump and the probe pulse as well as wave packet motions and the dynamic Stokes shift. Thus, only the decay-associated spectra (DAS) of the slower kinetic components are shown in Figure 4. The DAS of τ_2 shows strong contributions of excited state decay (centered around 460 and 590 nm) and stimulated emission (> 670 nm) as well as ground state recovery (around 510 nm) indicating a dominant transition from the excited state to the ground state potential energy surface. Additionally, a strong negative contribution around 540 nm indicates that the signature of the photoproduct is already formed with τ_2. In contrast, the DAS of τ_3 does not contain contributions of excited state depopulation and photoproduct formation but strongly resembles the DAS of τ_∞. Contributions of ground state recovery and a decaying early photoproduct signature centered around 590 nm are apparent. The DAS of τ_∞ reflects the $D75N_K$ − D75N difference spectrum.

Time-Resolved Measurements of NpSRII D75N with Azide. Analyzing the observed traces for D75N with azide (Figure 2B) in comparison to the one without azide (Figure 2A), the general spectral features do not change. Excited state absorption (region A), ground state bleaching (region B), photoproduct signature (region C), and stimulated emission (region D) are spectrally at

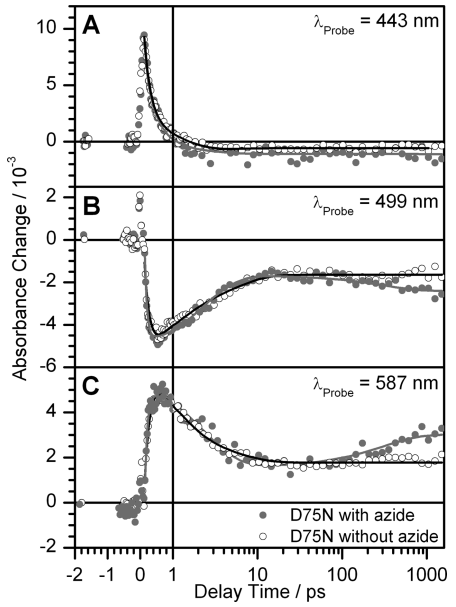

FIGURE 5: Transient absorbance changes of D75N with (shaded circle) and without (open circle) azide. Most prominent signals are related to the decay of the excited state (443 nm, A), the repopulation of the ground state (499 nm, B), and the formation of the photoproduct (587 nm, C).

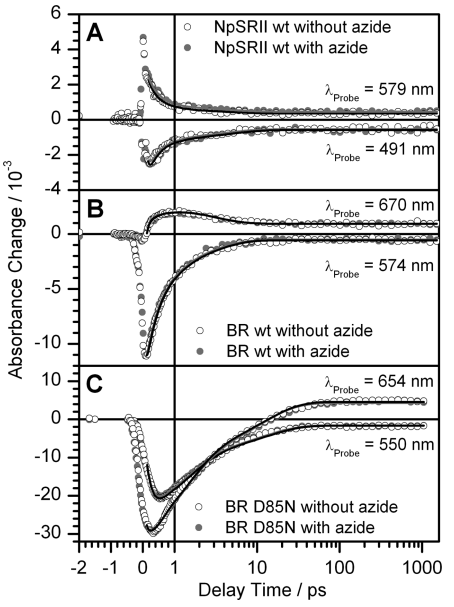

FIGURE 6: Transient absorbance changes depicting ground state bleaching and formation of the K intermediate for NpSRII wt (λ_{probe} = 491 nm and λ_{probe} = 579 nm, A), BR wt (λ_{probe} = 574 nm and λ_{probe} = 670 nm, B), and BR D85N (λ_{probe} = 550 nm and λ_{probe} = 654 nm, C) with (shaded circle) and without (open circle) azide, respectively.

the same position. Nevertheless, the global fitting routine reveals that the primary reaction is slightly accelerated by azide (Table 1; see also Figure 5A). The most striking difference however is the finding of two additional absorption features at delay times ≥100 ps; a negative absorption at 500 nm (Figure 5B) and a strong positive signal band around 570 nm (Figure 5C) become observable. It is thus evident that in the case of D75N containing azide an additional time constant in the range of 100 ps is needed to satisfactorily fit the data. The analysis of the transient absorbance changes using a global fitting routine reveals the following time constants: $\tau_1 \leq 0.15$ ps, $\tau_2 = 0.5$ ps, $\tau_3 = 3$ ps, $\tau_4 = 450$ ps, and $\tau_\infty = \infty$. The amplitudes of $\tau_1 - \tau_3$ and τ_∞ for D75N with and without azide exhibit similar spectral characteristics (Figure 4), which suggests an assignment of these time constants to the same processes. The DAS of the additionally emerging time constant τ_4 shows a negative contribution around 590 nm, indicating a growing signal in this wavelength range. The amplitudes in the other wavelength regions are negligible.

Time-Resolved Measurements of NpSRII wt. To confirm that the pronounced effect of azide is specific for the primary reaction dynamics of the NpSRII D75N mutant, a series of control measurements have been performed.

Time-dependent absorbance changes of NpSRII wt were recorded between 430 and 750 nm. Traces for selected probing wavelength are shown in Figure 6A. Around 500 nm an instantaneous absorption decrease caused by ground state depletion is observable. In the red wing of the ground state bleaching signal strong excited state absorption occurs at early times. The signal decays within 0.3 ps, followed by a further decrease on the picosecond time scale. At decay times >5 ps the residual signal stays constant. Weak negative signals indicative for stimulated emission are monitored at wavelengths above 700 nm, which also decay with a time constant of 0.3 ps. The data set is consistent with the one already published by Lutz et al. (*29*). The addition of 100 mM azide does not influence the reaction dynamics at all, which can be verified by a comparison of selected transients in Figure 6A.

Time-Resolved Measurements of BR wt. Transient absorbance changes were recorded as described above. Around 550 nm negative absorbance changes due to ground state depopulation appear. This signal shifts to shorter wavelengths during the first 10 ps and stays constant afterward. The signal arises within the apparatus response time and decays with 0.5 and 3 ps. Red shifted to the ground state signature photoproduct formation is visible at long delay times. At wavelengths >650 nm stimulated emission occurs and decays with the same time constant as the excited state absorption. The data agree with published work (*30*−*39*). No indication could be found that the primary reaction dynamics is influenced by azide, which becomes also evident from the transients given in Figure 6B.

Time-Resolved Measurements of BR D85N. The photoinduced transient difference spectra of BR D85N show a positive absorbance change due to the excited state absorption around 480 nm, which arises within the time resolution of the setup and decays on a 10 ps time scale. Around 550 nm negative absorbance changes indicative for ground state bleaching are observed. This band strongly overlaps with the signal from the K intermediate, leading to nearly complete cancellation of signals at delay times >15 ps. At the red-most end of the investigated spectral range negative contributions indicative for stimulated emission appear and decay with the same temporal behavior as the excited state absorption. The time constants derived by a global fitting procedure coincide with those received by transient absorption measurements of Logunov et al. (*34*). Also for the BR D85N mutant no influence on the reaction dynamics upon addition of azide could be found (Figure 6C).

DISCUSSION

In this paper the primary dynamics of NpSRII D75N and the influence of azide are investigated using transient absorption spectroscopy in the visible.

For NpSRII D75N without azide an ultrafast evolution on the S_1 surface within the first 150 fs is observed. In accordance to former investigations of retinal proteins (*26*, *29*, *37*, *39*−*41*) this process is attributed to a wave packet motion out of the Franck−Condon region. It is widely discussed to be an in-plane stretching motion of the conjugated carbon chain, which is followed by a torsional motion around the C_{13}=C_{14} double bond. The relayed excited state population afterward decays monoexponentially with 0.8 ps populating both the all-*trans* retinal ground state and a photoproduct state absorbing around 590 nm. In analogy to NpSRII wt (*29*) the photoproduct is assigned to the K intermediate characterized by an isomerized 13-*cis*-retinal. The DAS of the subsequent time constant of 3.5 ps leads to the conclusion that part of the population of the early photoproduct evolves to the all-*trans* ground state. The DAS of τ_∞ reflects the $D75N_K$ − D75N difference spectrum.

Comparing these findings to the results obtained for NpSRII wt (*29*), two main differences emerge upon Asp to Asn replacement. First, the time constant associated with the fast decay of the excited electronic state increases by more than a factor of 2 from 0.3 (*29*) to 0.8 ps. This overall slower response upon removal of the primary proton acceptor is a well-known feature for retinal proteins and is thought to be caused by changed electrostatics associated with altered hydrogen-bonding networks (*25*, *33*, *42*−*45*). For proteorhodopsin (PR) it was shown that the protonation state of the primary proton acceptor has already a strong impact on the reaction rates (*26*, *40*, *46*, *47*). Within the framework of potential energy surfaces the pH-dependent differences were rationalized as a tilting of the S_1 surface. However, electrostatic interactions also affect the shape of potential energy surfaces and the character of the wave function as calculated for BR (*48*). For BR D85T it was proposed that the mutation introduces a barrier in the S_1 potential which affects the accessibility of a conical intersection thus influencing the reaction rates (*49*). Further arguments were proposed by El-Sayed et al. (*44*), who discussed Asp85 and Asp212 in BR to be necessary for tightening the retinal binding pocket, thus introducing an anisotropic potential with specific repulsion which would facilitate ultrafast isomerization. Isomerization would be retarded if the mutation weakens or deletes this potential. The importance of water in the associated hydrogen-bonding network has been discussed widely (*45*, *50*, *51*). The overall belief is that a mutation of the primary proton acceptor perturbs the stabilizing geometry, destabilizes the active site, and therefore influences the isomerization dynamics as well.

The second difference between NpSRII wt and the D75N mutant becomes evident by looking at the transient absorbance changes at different delay times. Whereas a clear stationary point is observable in the wt data, this characteristic point is absent in the traces for the D75N mutant (Figure 3A,B). The decay of the excited state can therefore not be described by a simple two-state model as proposed by Lutz et al. (*29*). As both Losi et al. (*14*) and Inoue et al. (*13*) showed that multiple optically silent K intermediates are present in the photocycle of NpSRII D75N, we propose that at least two K states are populated via the excited state decay, termed K_1 and K_2. According to the literature (*13*, *14*) the K_1 to K_2 transition proceeds on a 100 ns time scale.

Concerning the investigation of the D75N mutant with azide, it could be shown that the addition of this external anion does not have a great impact on the general optical properties, e.g., electronic transitions (see Figures 1 and 2), but produces a pronounced effect on the reaction dynamics. On the one hand the reaction kinetics are slightly accelerated. This can be best seen in the comparison of time constants obtained by the global fit ($\tau_2 = 0.8$ ps and $\tau_3 = 3.5$ ps for D75N; $\tau_2 = 0.5$ ps and $\tau_3 = 3.0$ ps for D75N azide; see Table 1) and the transients for single wavelengths depicted in Figure 5A−C. We attribute this to the fact that at physiological pH negatively charged N_3^- ions have a great impact on the hydrogen-bonding network (*22*), presumably restoring part of the negative charge at the position of the counterion of the Schiff base. Further on, two additional absorption features at delay times ≥100 ps connected to a further transition in the 100 ps time range become clearly observable. The observed signals at long delay times can be explained under the assumption that azide accelerates the transition of K_1 to K_2 by at least 1 order of magnitude, becoming thus visible in the time range investigated here. Although in principle the assumption of two K intermediates agree with the results obtained by Losi et al. (*14*) and Inoue et al. (*13*), the photoproducts observed in this study are not optically silent, since there are contributions at 500 nm as well as around 570 nm. We suppose K_2 to absorb slightly red shifted compared to K_1.

As NpSRII wt is not responsive toward azide, it seems that the structural properties in the vicinity of the retinal differ drastically for NpSRII wt and D75N. It is not unlikely to assume that the D75N mutant exhibits a different hydrogen-bonding pattern, which reacts very sensitively to the addition of azide. This is further in agreement with static low temperature and step scan FTIR measurements of Hein et al. (*52*). They found that the amide I band changes and the temperature-dependent photoproduct yield differs considerably for sensory rhodopsin wt and D75N. They attribute this to the fact that the dark states of sensory rhodopsin wt and the D75N mutant have different structures.

Since both BR and the respective counterion mutant D85N are not at all sensitive toward azide (Figure 6B,C), the characteristic influence of azide on the primary reaction of NpSRII D75N is likely to be a unique feature of this mutant. Under the assumption that the formation of the signaling state is directly coupled to the structural rearrangements after retinal isomerization, the observed influence of the neutralization of the Schiff base counterion verifies the functional importance of this residue.

REFERENCES

1. Oesterhelt, D., and Stoeckenius, W. (1971) Rhodopsin-like protein from purple membrane of *Halobacterium halobium*. *Nat. New Biol. 233*, 149.
2. Oesterhelt, D. (1998) The structure and mechanism of the family of retinal proteins from halophilic archaea. *Curr. Opin. Struct. Biol. 8*, 489–500.
3. Kolbe, M., Besir, H., Essen, L. O., and Oesterhelt, D. (2000) Structure of the light-driven chloride pump halorhodopsin at 1.8 angstrom resolution. *Science 288*, 1390–1396.
4. Bamberg, E., Tittor, J., and Oesterhelt, D. (1993) Light-driven proton or chloride pumping by halorhodopsin. *Proc. Natl. Acad. Sci. U.S.A. 90*, 639–643.
5. Spudich, J. L. (1993) Color sensing in the archaea—a eukaryotic-like receptor-coupled to a prokaryotic transducer. *J. Bacteriol. 175*, 7755–7761.
6. Royant, A., Nollert, P., Edman, K., Neutze, R., Landau, E. M., Pebay-Peyroula, E., and Navarro, J. (2001) X-ray structure of sensory rhodopsin II at 2.1-angstrom resolution. *Proc. Natl. Acad. Sci. U.S.A. 98*, 10131–10136.

7. Hohenfeld, I. P., Wegener, A. A., and Engelhard, M. (1999) Purification of histidine tagged bacteriorhodopsin, pharaonis halorhodopsin and pharaonis sensory rhodopsin II functionally expressed in *Escherichia coli*. *FEBS Lett. 442*, 198–202.
8. Sasaki, J., and Spudich, J. L. (2008) Signal transfer in haloarchaeal sensory rhodopsin-transducer complexes. *Photochem. Photobiol. 84*, 863–868.
9. Klare, J. P., Bordignon, E., Doebber, M., Fitter, J., Kriegsmann, J., Chizhov, I., Steinhoff, H. J., and Engelhard, M. (2006) Effects of solubilization on the structure and function of the sensory rhodopsin II/transducer complex. *J. Mol. Biol. 356*, 1207–1221.
10. Klare, J. P., Bordignon, E., Engelhard, M., and Steinhoff, H. J. (2004) Sensory rhodopsin II and bacteriorhodopsin: Light activated helix F movement. *Photochem. Photobiol. Sci. 3*, 543–547.
11. Moukhametzianov, R., Klare, J. P., Efremov, R., Baeken, C., Goppner, A., Labahn, J., Engelhard, M., Büldt, G., and Gordeliy, V. I. (2006) Development of the signal in sensory rhodopsin and its transfer to the cognate transducer. *Nature 440*, 115–119.
12. Friedrich, T., Geibel, S., Kalmbach, R., Chizhov, I., Ataka, K., Heberle, J., Engelhard, M., and Bamberg, E. (2002) Proteorhodopsin is a light-driven proton pump with variable vectoriality. *J. Mol. Biol. 321*, 821–838.
13. Inoue, K., Sasaki, J., Spudich, J. L., and Terazima, M. (2007) Laser-induced transient grating analysis of dynamics of interaction between sensory rhodopsin II D75N and the HtrII transducer. *Biophys. J. 92*, 2028–2040.
14. Losi, A., Wegener, A. A., Engelhard, M., Gärtner, W., and Braslavsky, S. E. (2000) Aspartate 75 mutation in sensory rhodopsin II from *Natronobacterium pharaonis* does not influence the production of the K-like intermediate, but strongly affects its relaxation pathway. *Biophys. J. 78*, 2581–2589.
15. Sasaki, J., Nara, T., Spudich, E. N., and Spudich, J. L. (2007) Constitutive activity in chimeras and deletions localize sensory rhodopsin II/HtrII signal relay to the membrane-inserted domain. *Mol. Microbiol. 66*, 1321–1330.
16. Schmies, G., Luttenberg, B., Chizhov, I., Engelhard, M., Becker, A., and Bamberg, E. (2000) Sensory rhodopsin II from the haloalkaliphilic *Natronobacterium pharaonis*: Light-activated proton transfer reactions. *Biophys. J. 78*, 967–976.
17. Yang, C. S., Sineshchekov, O., Spudich, E. N., and Spudich, J. L. (2004) The cytoplasmic membrane-proximal domain of the HtrII transducer interacts with the E-F loop of photoactivated *Natronomonas pharaonis* sensory rhodopsin II. *J. Biol. Chem. 279*, 42970–42976.
18. Tittor, J., Soell, C., Oesterhelt, D., Butt, H. J., and Bamberg, E. (1989) A defective proton pump, point-mutated bacteriorhodopsin Asp96Asn is fully reactivated by azide. *EMBO J. 8*, 3477–3482.
19. Tittor, J., Wahl, M., Schweiger, U., and Oesterhelt, D. (1994) Specific acceleration of deprotonation and reprotonation steps by azide in mutated bacteriorhodopsins. *Biochim. Biophys. Acta 1187*, 191–197.
20. Cao, Y., Varo, G., Chang, M., Ni, B. F., Needleman, R., and Lanyi, J. K. (1991) Water is required for proton-transfer from aspartate-96 to the bacteriorhodopsin Schiff-base. *Biochemistry 30*, 10972–10979.
21. Takao, K., Kikukawa, T., Araiso, T., and Kamo, N. (1998) Azide accelerates the decay of M-intermediate of *pharaonis* phoborhodopsin. *Biophys. Chem. 73*, 145–153.
22. Le Coutre, J., Tittor, J., Oesterhelt, D., and Gerwert, K. (1995) Experimental evidence for hydrogen-bonded network proton-transfer in bacteriorhodopsin shown by Fourier-transform infrared-spectroscopy using azide as catalyst. *Proc. Natl. Acad. Sci. U.S.A. 92*, 4962–4966.
23. Steinhoff, H. J., Pfeiffer, M., Rink, T., Burlon, O., Kurz, M., Riesle, J., Heuberger, E., Gerwert, K., and Oesterhelt, D. (1999) Azide reduces the hydrophobic barrier of the bacteriorhodopsin proton channel. *Biophys. J. 76*, 2702–2710.
24. Tittor, J., Schweiger, U., Oesterhelt, D., and Bamberg, E. (1994) Inversion of proton translocation in bacteriorhodopsin mutants D85N, D85T, and D85,96N. *Biophys. J. 67*, 1682–1690.
25. Riedle, E., Beutter, M., Lochbrunner, S., Piel, J., Schenkl, S., Sporlein, S., and Zinth, W. (2000) Generation of 10 to 50 fs pulses tunable through all of the visible and the NIR. *Appl. Phys. 71*, 457–465.
26. Huber, R., Köhler, T., Lenz, M. O., Bamberg, E., Kalmbach, R., Engelhard, M., and Wachtveitl, J. (2005) pH-dependent photoisomerization of retinal in proteorhodopsin. *Biochemistry 44*, 1800–1806.
27. Mogi, T., Stern, L. J., Marti, T., Chao, B. H., and Khorana, H. G. (1988) Structure-function studies on bacteriorhodopsin. Aspartic-acid substitutions affect proton translocation by bacteriorhodopsin. *Proc. Natl. Acad. Sci. U.S.A. 85*, 4148–4152.
28. Subramaniam, S., Marti, T., and Khorana, H. G. (1990) Protonation state of Asp (Glu)-85 regulates the purple-to-blue transition in bacteriorhodopsin mutants Arg-82 → Ala and Asp-85 → Glu: The blue form is inactive in proton translocation. *Proc. Natl. Acad. Sci. U.S.A. 87*, 1013–1017.
29. Lutz, I., Sieg, A., Wegener, A. A., Engelhard, M., Boche, I., Otsuka, M., Oesterhelt, D., Wachtveitl, J., and Zinth, W. (2001) Primary reactions of sensory rhodopsins. *Proc. Natl. Acad. Sci. U.S.A. 98*, 962–967.
30. Blanchard, D., Gilmore, D. A., Brack, T. L., Lemaire, H., Hughes, D., and Atkinson, G. H. (1991) Picosecond time-resolved absorption and fluorescence in the bacteriorhodopsin photocycle—vibrationally-excited species. *Chem. Phys. 154*, 155–170.
31. Dobler, J., Zinth, W., Kaiser, W., and Oesterhelt, D. (1988) Excited-state reaction dynamics of bacteriorhodopsin studied by femtosecond spectroscopy. *Chem. Phys. Lett. 144*, 215–220.
32. Haacke, S., Schenkl, S., Vinzani, S., and Chergui, M. (2002) Femtosecond and picosecond fluorescence of native bacteriorhodopsin and a nonisomerizing analog. *Biopolymers 67*, 306–309.
33. Heyne, K., Herbst, J., Dominguez-Herradon, B., Alexiev, U., and Diller, R. (2000) Reaction control in bacteriorhodopsin: Impact of Arg82 and Asp85 on the fast retinal isomerization, studied in the second site revertant Arg82Ala/Gly231Cys and various purple and blue forms of bacteriorhodopsin. *J. Phys. Chem. 104*, 6053–6058.
34. Logunov, S. L., ElSayed, M. A., Song, L., and Lanyi, J. K. (1996) Photoisomerization quantum yield and apparent energy content of the K intermediate in the photocycles of bacteriorhodopsin, its mutants D85N, R82Q, and D212N, and deionized blue bacteriorhodopsin. *J. Phys. Chem. 100*, 2391–2398.
35. Logunov, S. L., Volkov, V. V., Braun, M., and El-Sayed, M. A. (2001) The relaxation dynamics of the excited electronic states of retinal in bacteriorhodopsin by two-pump-probe femtosecond studies. *Proc. Natl. Acad. Sci. U.S.A. 98*, 8475–8479.
36. Mathies, R. A., Cruz, C. H. B., Pollard, W. T., and Shank, C. V. (1988) Direct observation of the femtosecond excited-state cis-trans isomerization in bacteriorhodopsin. *Science 240*, 777–779.
37. Schenkl, S., van Mourik, F., Friedman, N., Sheves, M., Schlesinger, R., Haacke, S., and Chergui, M. (2006) Insights into excited-state and isomerization dynamics of bacteriorhodopsin from ultrafast transient UV absorption. *Proc. Natl. Acad. Sci. U.S.A. 103*, 4101–4106.
38. Sharkov, A. V., Pakulev, A. V., Chekalin, S. V., and Matveetz, Y. A. (1985) Primary events in bacteriorhodopsin probed by subpicosecond spectroscopy. *Biochim. Biophys. Acta 808*, 94–102.
39. Wang, J. P., Link, S., Heyes, C. D., and El-Sayed, M. A. (2002) Comparison of the dynamics of the primary events of bacteriorhodopsin in its trimeric and monomeric states. *Biophys. J. 83*, 1557–1566.
40. Neumann, K., Verhoefen, M. K., Weber, I., Glaubitz, C., and Wachtveitl, J. (2008) Initial reaction dynamics of proteorhodopsin observed by femtosecond infrared and visible spectroscopy. *Biophys. J. 94*, 4796–4807.
41. Arlt, T., Schmidt, S., Zinth, W., Haupts, U., and Oesterhelt, D. (1995) The initial reaction dynamics of the light-driven chloride pump halorhodopsin. *Chem. Phys. Lett. 241*, 559–565.
42. Lenz, M. O., Woerner, A. C., Glaubitz, C., and Wachtveitl, J. (2007) Photoisomerization in proteorhodopsin mutant D97N. *Photochem. Photobiol. 83*, 226–231.
43. Garczarek, F., and Gerwert, K. (2006) Functional waters in intraprotein proton transfer monitored by FTIR difference spectroscopy. *Nature 439*, 109–112.
44. El-Sayed, M. A., Griffiths, J., Song, L., and Zhang, N. (1995) On the molecular mechanisms of the rapid and slow solar-to-electric energy-storage processes by the other natural photosynthetic system, bacteriorhodopsin. *Pure Appl. Chem. 67*, 149–155.
45. Baudry, J., Tajkhorshid, E., Molnar, F., Phillips, J., and Schulten, K. (2001) Molecular dynamics study of bacteriorhodopsin and the purple membrane. *J. Phys. Chem. 105*, 905–918.
46. Lenz, M. O., Huber, R., Schmidt, B., Gilch, P., Kalmbach, R., Engelhard, M., and Wachtveitl, J. (2006) First steps of retinal photoisomerization in proteorhodopsin. *Biophys. J. 91*, 255–262.
47. Verhoefen, M. K., Neumann, K., Weber, I., Glaubitz, C., and Wachtveitl, J. (2009) Primary reaction dynamics of proteorhodopsin mutant D97N observed by femtosecond infrared and visible spectroscopy. *Photochem. Photobiol. 85*, 540–546.
48. Nonella, M. (2000) Electrostatic protein-chromophore interactions promote the all-trans → 13-cis isomerization of the protonated retinal Schiff base in bacteriorhodopsin: An ab initio CASSCF/MRCI study. *J. Phys. Chem. 104*, 11379–11388.
49. Zinth, W., Sieg, A., Huppmann, P., Blankenhorn, T., Oesterhelt, D., and Nonella, M. (2001) Femtosecond spectroscopy and model

calculations for an understanding of the primary reaction in bacteriorhodopsin, in Ultrafast Phenomena XII (Elsaesser, T., Mukamel, S., Murnane, M. M., and Scherer, N. F., Eds.) pp 680−682, Springer, Berlin/Heidelberg/New York.
50. Herbst, J., Heyne, K., and Diller, R. (2002) Femtosecond infrared spectroscopy of bacteriorhodopsin chromophore isomerization. *Science 297*, 822–825.
51. Luecke, H., Schobert, B., Richter, H. T., Cartailler, J. P., and Lanyi, J. K. (1999) Structure of bacteriorhodopsin at 1.55 angstrom resolution. *J. Mol. Biol. 291*, 899–911.
52. Hein, M., Radu, I., Klare, J. P., Engelhard, M., and Siebert, F. (2004) Consequences of counterion mutation in sensory rhodopsin II of *Natronobacterium pharaonis* for photoreaction and receptor activation: An FTIR study. *Biochemistry 43*, 995–1002.